ELSEVIER

International Journal of Heat and Fluid Flow 20 (1999) 520–529

International Journal of HEAT AND FLUID FLOW

www.elsevier.com/locate/ijhff

CFD analysis of spray propagation and evaporation including wall film formation and spray/film interactions

R. Schmehl *, H. Rosskamp, M. Willmann, S. Wittig

Institut für Thermische Strömungsmaschinen, Universität Karlsruhe, Kaiserstraße 12, 76128 Karlsruhe, Germany

Abstract

Addressing the numerical simulation of complex two-phase flows in gas turbine combustors, this study features a comprehensive approach to the coupled solution of the interacting flow fields of the gas phase, evaporating fuel spray and evaporating, shear-driven fuel wall film. The gas flow and wall-film flow are described in Eulerian coordinates and are both calculated in the same computational unit. A second, separate program is based on Lagrangian particle tracking to model spray dispersion and evaporation. To account for interaction effects, an iterative procedure is applied considering mutual mass, momentum and energy transfer between the three flow regimes. For a realistic modeling of spray/wall and spray/film interaction, the droplet-trajectory computation comprises a set of droplet-impact models covering a broad range of impact conditions. The results of a two-phase flow simulation in a schematic LPP combustor premix duct demonstrate the effects of phase interaction as well as spray/wall and spray/film interaction. © 1999 Elsevier Science Inc. All rights reserved.

Keywords: Sprays; Evaporation; CFD; Films; Droplet-trajectories

Notation

a	coefficient
cfm	correction factor for mass transport
cfh	correction factor for energy transport
c_p	specific heat capacity (J/(kg K))
c_W	aerodynamic drag coefficient
D	diameter (m)
h_f	average film thickness (m)
h^*	non-dimensional film thickness
h_v	evaporation enthalpy (J/kg)
k	turbulent kinetic energy (m^2/s^2)
k_s	equivalent sandgrain roughness (m)
La	Laplace number
Le	Lewis number
$\dot{m}_f^*$	fuel film mass flux per unit width (kg/(s m))
On	Ohnesorge number
Pr	Prandtl number
Re	Reynolds number
r_a	radius of the duct (m)
S	splashing parameter, source term
Sc	Schmidt number
Tr	droplet rate (1/s)
U^{**}	circumferential shear velocity scale
u, v, w	velocity components (m/s)
u_τ	shear stress velocity (m/s)
V_c	liquid volume concentration
W^{**}	axial shear velocity scale
We	Weber number
Y	mass fraction
y, z	radial, axial coordinate (m)
α	impact angle (rad), relaxation factor (−)
ε	turbulent dissipation rate (m^2/s^3)
Γ	general diffusion coefficient
Γ_{im}	effective diffusion coefficient (m^2/s)
κ	mixing length constant
η	deposition rate
μ	dynamic viscosity (Pa s)
ρ	density (kg/m^3)
σ	surface tension, variance (N/m)
τ_w	wall shear stress (N/m^2)
Φ	equivalence ratio
φ	circumferential coordinate
ϕ	general transport variable

Subscripts

b	boiling
g, f, d	gas, film, droplet
L	Leidenfrost
m	mean
ref	reference
s	droplet surface
vap	vapor
w	wall

1. Introduction

Computational fluid dynamics of single- and two-phase flows in combustors has been a rapidly developing research

* Corresponding author. E-mail: roland.schmehl@mach.uni-karlsruhe.de

0142-727X/99/$ – see front matter © 1999 Elsevier Science Inc. All rights reserved.
PII: S0142-727X(99)00041-7

topic over the last years. Especially, design and optimization of advanced, low-emission combustors are based on numerical simulations to a growing extent. In these combustor designs, performance and reliability significantly depend on local flow phenomena. At this point, advanced CFD codes are a valuable complement to experimental investigations, since they allow a detailed local analysis of the flow. Engineering flow prediction of single-phase flows is a standard application of CFD and widely used nowadays. In the same way, the computation of spray dispersion and evaporation has been developed into a practicable prediction tool (Tolpadi et al., 1995; Tolpadi, 1995; Kurreck et al., 1996). Even though advanced models have been developed (Witting et al., 1991), the numerical prediction of evaporating shear-driven wall films has still been limited to special geometries or flow cases (Baumann et al., 1989). The numerical simulation of complex, two-phase flows in combustors with evaporating fuel sprays and wall films is a challenge for many years now. However, attempts to consider the interaction of gas flow, spray and wall film have been stagnating due to a lack of practicable models for spray/wall and spray/film interaction as well as wall-film propagation. Based on extensive experimental research, reliable and validated models accomplishing these demands have recently been proposed by Rosskamp et al. (1997) and Samenfink (1997).

2. Numerical approach

In the fuel/air mixing region the combustor flow is determined by phase interaction effects and in the case of premixing ducts or air-blast nozzles by spray/wall and spray/film interaction. Fig. 1 gives an overview of the two-phase flow phenomenain a schematic premix duct of a Lean Premix Prevaporize (LPP) combustor. A pressure atomizer ejects the droplet spray into the hot compressor air flow where it is dispersed and evaporated. The gas flow in turn is affected by evaporation cooling and aerodynamic acceleration due to the spray. The liquid wall film is fed either directly onto the wall or it is built up by deposition of droplets. In both cases, gas flow and film flow are coupled by mass, momentum and energy transfer due to film evaporation and surface shear stress. Depending on the impact parameters, droplet impact on the duct wall or the wall film may result in deposition, splashing, reflection or spontaneous evaporation of the droplet. These wall effects have a significant influence on the vapor concentration in the near-wall flow region. The numerical approach presented in this study is based on an Eulerian description of the gas and film flow and a Lagrangian description of spray dispersion and evaporation. The gas flow and film flow are simultaneously calculated in the program EPOS, applying a 3D finite volume discretization and a linear system solver for the gas flow and a 2D Finite Difference scheme combined with a Runge–Kutta solver for the film flow. Based on the gas-phase flow field and film data, spray dispersion and evaporation is calculated in a second individual program, Ladrop (see Fig. 2). The trajectory approach for the spray has been chosen, because of its inherent suitability for the modeling of complex technical sprays characterized by a broad range of droplet initial conditions and droplet/wall interactions. Interaction between the flow regimes' gas flow, film flow and spray is realized by arranging the programs EPOS and Ladrop in an iteration loop. The reaction of gas and film flow upon the spray due to evaporation cooling, aerodynamic acceleration or film build up by droplet deposition is taken into account by considering droplet source term fields computed in Ladrop in the following gas and film flow calculation by EPOS.

3. Gas flow

The computation of the turbulent, three-dimensional gas flow field is done with the computer program EPOS, developed

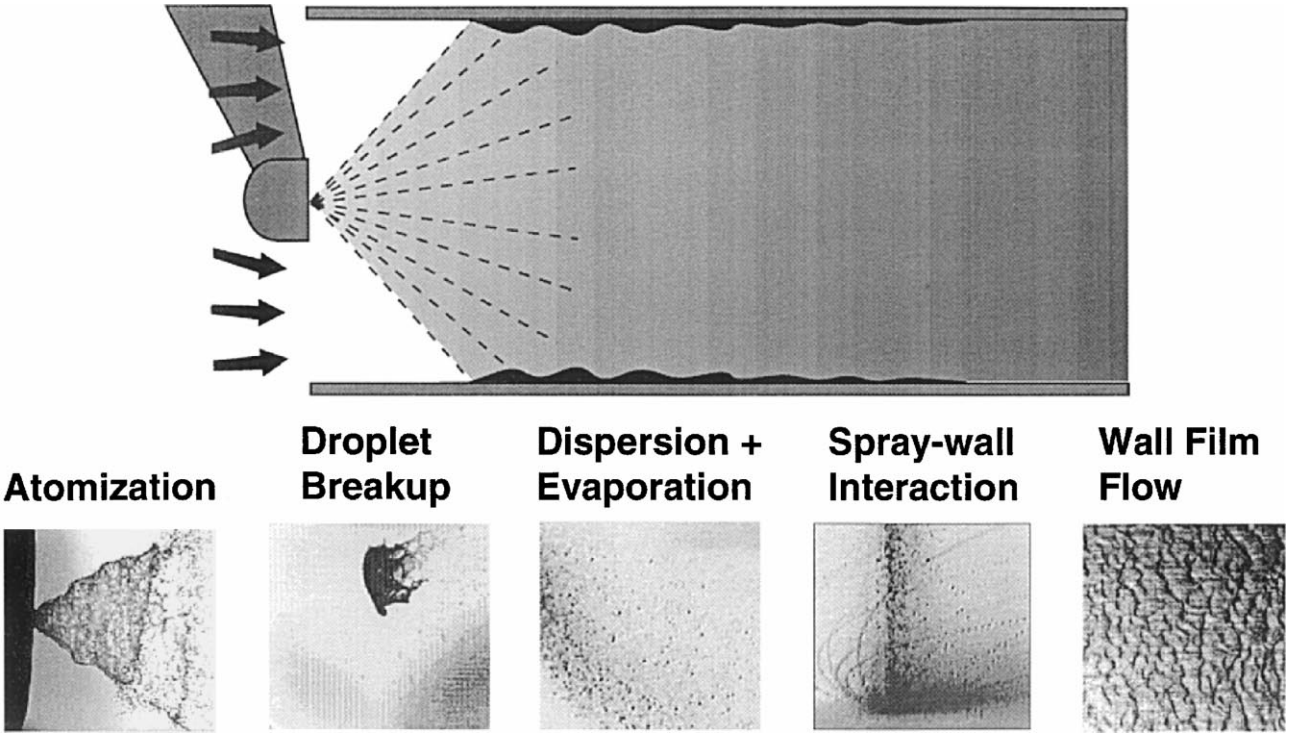

Fig. 1. Two-phase flow phenomena in the premix duct.

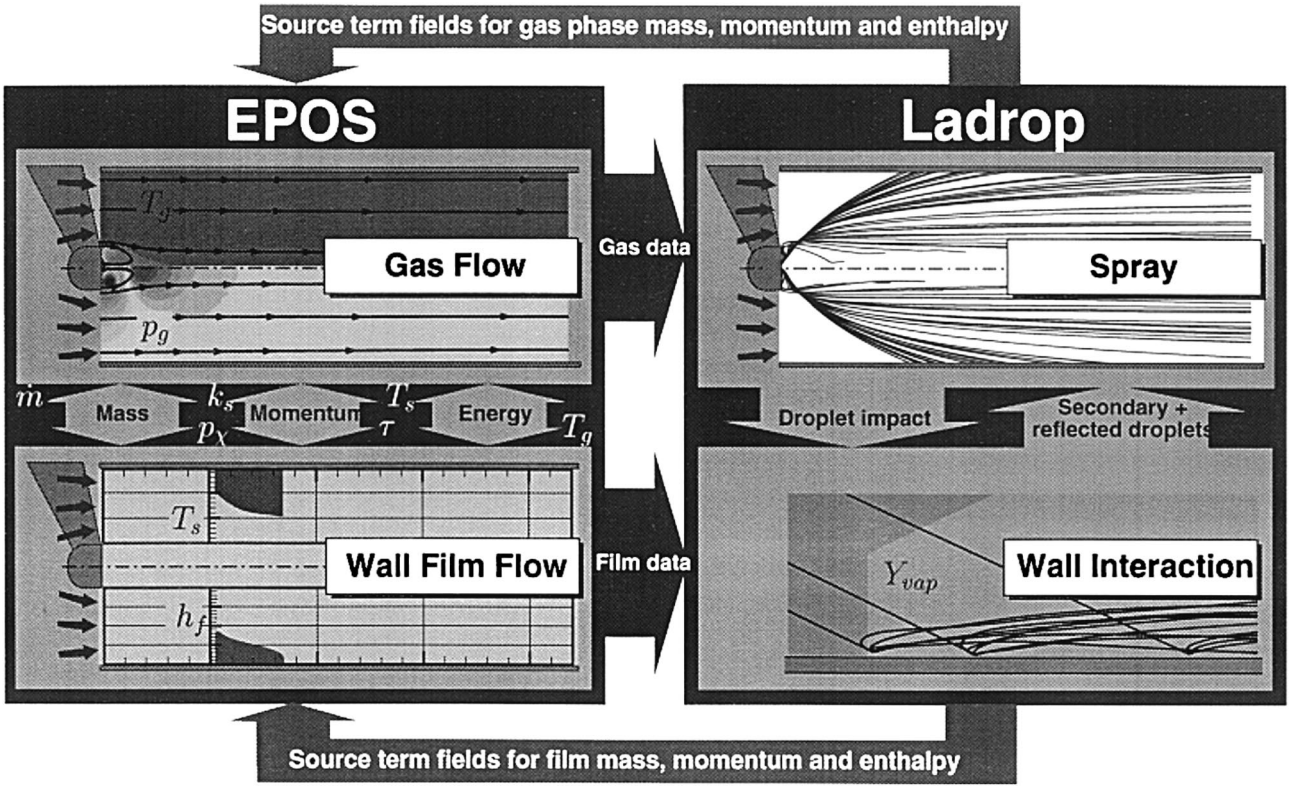

Fig. 2. Coupled calculation of the two-phase flow with EPOS and Ladrop.

at the Institut für Thermische Strömungsmaschinen. EPOS is based on the Reynolds-averaged Navier–Stokes equations represented by the general formulation for flow variable ϕ

$$\operatorname{div}(\rho\vec{u}\phi) = \operatorname{div}(\Gamma_\phi \operatorname{grad}\phi) + S_\phi. \tag{1}$$

In this equation, Γ_ϕ is an effective diffusion coefficient and S_ϕ comprises local sources. Possible substitutions for ϕ are 1, resulting in the continuity equation, or u, v, w, h and Y_{vap}. The standard k–ε turbulence model is included by solving two additional transport equations for the turbulent kinetic energy k and its dissipation rate ε (Launder and Spalding, 1974). The system of transport equations is formulated in a cylindrical coordinate system and discretized by means of a finite-volume method. The coupled velocity–pressure field is determined using the SIMPLEC pressure-correction algorithm on non-staggered grids as described by Van Doormal and Raithby (1984). The temperature distribution is derived from the enthalpy field and the density is calculated from an equation of state for an ideal mixture. The finite-volume balance equations are arranged in septdiagonal matrix form,

$$\begin{gathered} a_P\phi_P = \sum_{nb} a_{nb}\phi_{nb} + S_\phi, \quad a_P = \sum_{nb} a_{nb} + S_m, \\ nb = E, W, N, S, H, L, \end{gathered} \tag{2}$$

which are solved by an iterative solution procedure based on a conjugate gradient method (Noll et al., 1991). In the presence of a liquid wall film, special wall functions have to be applied to represent the flow in the near-wall region correctly. The film surface is considered to be a rough, moving wall with negligible velocity. Additionally, the curvature of the wall must be taken into account for a precise prediction of wall shear stress and interfacial shear stress, respectively. The wall shear stress is computed in two components (aligned with the axis and along the curved wall, respectively) according to the following equations (Kind et al., 1989)

$$\frac{w}{W^{**}} = \frac{1}{\kappa}\ln\left(\frac{yW^{**}}{v}\right) + C, \tag{3}$$

$$\frac{u}{U^{**}} = \left(1 - \frac{y}{r_a}\right)\left[\frac{1}{\kappa}\ln\left(\frac{yU^{**}}{v(1-y/r_a)}\right) + C\right], \tag{4}$$

where the shear velocity scales are defined as

$$U^{**} = \sqrt{\frac{\tau_{w,\varphi}^2}{\rho\tau_w}}, \qquad W^{**} = \sqrt{\frac{\tau_{w,z}}{\rho\tau_w}}. \tag{5}$$

C denotes a constant which has to be chosen according to the roughness of the wall or the film surface,respectively. Three different regimes identified in terms of the roughness Reynolds number $\mathrm{Re}_{k_s} = u_\tau k_s/v$ have to be considered (Kays and Crawford, 1980, Himmelsbach et al., 1994)

- *Hydraulically smooth surface*, $\mathrm{Re}_{k_s} \leqslant 5.0$:

$$C(\mathrm{Re}_{k_s}) = 5.15. \tag{6}$$

- *Slightly rough surface*, $5.0 < \mathrm{Re}_{k_s} \leqslant 70.0$:

$$C(\mathrm{Re}_{k_s}) = 1.5497 + 19.1\log\mathrm{Re}_{k_s} - 14.4339\log^2\mathrm{Re}_{k_s} + 3.30869\log^3\mathrm{Re}_{k_s} - \frac{1}{\kappa}\ln\mathrm{Re}_{k_s}. \tag{7}$$

- *Rough surface*, $\mathrm{Re}_{k_s} \geqslant 70.0$:

$$C(\mathrm{Re}_{k_s}) = 8.5 - \frac{1}{\kappa}\ln\mathrm{Re}_{k_s}. \tag{8}$$

For the computation of heat transfer, the analogy of momentum and heat transfer is used. Mass exchange is also

computed making use of this analogy. However, in the case of rough surfaces the analogy suffers from one defect: whereas the momentum exchange shifts from molecular mechanisms to more macroscale drag forces with increasing roughness, the heat and mass transfer is always limited to molecular mechanisms close to the surface. This phenomenon is taken into account by means of a correction term which has been proposed for shear driven films by Sill (1982) and Himmelsbach et al. (1994).

4. Spray dispersion and evaporation

The Lagrangian method is based on the tracking of individual droplets in the gas-phase flow field by integrating their equation of motion combined with an empirical correlation for the aerodynamic drag coefficient given by Stein (1973)

$$\frac{\mathrm{d}\vec{u}_\mathrm{d}}{\mathrm{d}t} = -\frac{3}{4}\frac{\rho_\mathrm{g}}{\rho_\mathrm{d}}\frac{c_\mathrm{W}}{D}\,|\,\vec{u}_\mathrm{d}-\vec{u}_\mathrm{g}\,|\,(\vec{u}_\mathrm{d}-\vec{u}_\mathrm{g}),$$
$$c_\mathrm{W} = 0.36 + 5.48\mathrm{Re}_\mathrm{d}^{-0.573} + \frac{24}{\mathrm{Re}_\mathrm{d}}. \tag{9}$$

In order to simulate the effect of turbulent spray dispersion, the gas velocity is randomly sampled along the trajectories according to the approach of Gosman and Ioannides (1983). In this concept, characteristic quantities of the turbulence structure are determined from mean gas flow properties. Specifically, the length scale l_e and dissipation time scale t_e of the idealized eddies are calculated from local turbulence properties as follows

$$l_\mathrm{e} = C_\mu^{1/2}\frac{k^{3/2}}{\varepsilon}, \qquad t_\mathrm{e} = \sqrt{\frac{3}{2}}\,C_\mu^{1/2}\,\frac{k}{\varepsilon}. \tag{10}$$

In addition to the life time scale t_e, the droplet dynamics are taken into account in the following integral relation for the crossing time scale t_c

$$\left|\int_{t_0}^{t_\mathrm{c}} (\vec{u}_\mathrm{g}-\vec{u}_\mathrm{d})\,\mathrm{d}t\right| = l_\mathrm{e}. \tag{11}$$

When the smaller of these time scales has elapsed, the droplet is deemed to enter a new eddy. Consequently, the random process generates a new velocity fluctuation $\vec{u}'_g$ from a Gaussian distribution determined by

$$\mu = 0, \quad \sigma = \sqrt{\frac{2}{3}k}. \tag{12}$$

The model constant C_μ in Eq. (10) has a decisive influence on the dispersion behavior of the turbulent spray. The most realistic results have been obtained by choosing the value 0.09 (Milojević, 1990). With respect to spray evaporation, the Uniform Temperature model is used in this approach. This computationally effective model is based on the assumption of a homogeneous temperature distribution in the droplet and phase equilibrium conditions at the liquid/gas interface. In the gas phase around the droplet, diffusive time scales are smaller by orders of magnitude giving rise to a quasi-stationary description of the diffusive transport processes. Using reference values for variable fluid properties (1/3-rule of Sparrow and Gregg, 1958), an integration of the radial symmetric differential equations yields analytical expressions for the diffusive transport fluxes. Convective transport is accounted for by two empirical correction factors cfm and cfh resulting in the following balance equations for droplet mass and temperature

$$\frac{\mathrm{d}m_\mathrm{d}}{\mathrm{d}t} = -\,\mathrm{cfm}\;2\pi D\;\rho_{\mathrm{g,ref}}\;\Gamma_{\mathrm{im,ref}}\ln\frac{1-Y_{\mathrm{vap,g}}}{1-Y_{\mathrm{vap,s}}}, \tag{13}$$

$$\frac{\mathrm{d}T_\mathrm{d}}{\mathrm{d}t} = -\frac{1}{m_\mathrm{d}c_{\mathrm{p,d}}}\frac{\mathrm{d}m_\mathrm{d}}{\mathrm{d}t}\left[\frac{\mathrm{cfh}}{\mathrm{cfm}}c_{\mathrm{p,vap,ref}}(T_\mathrm{g}-T_\mathrm{d})\cdot\right.$$
$$\left.\times\left(\left[\frac{1-Y_{\mathrm{vap,g}}}{1-Y_{\mathrm{vap,s}}}\right]^{1/\mathrm{Le}}-1\right)^{-1}-h_\mathrm{v}\right],$$

$$\mathrm{cfm} = 1+0.276\mathrm{Re}^{1/2}\,\mathrm{Sc}^{1/3}, \quad \mathrm{cfh} = 1+0.276\mathrm{Re}^{1/2}\,\mathrm{Pr}^{1/3}. \tag{14}$$

In these equations, $Y_{\mathrm{vap,s}}$ is the vapor concentration at the droplet surface, whereas T_g and $Y_{\mathrm{vap,g}}$ represent free stream values. Variable fluid properties are determined by correlations. The resulting system of coupled ordinary differential equations describing the motion and evaporation of individual droplets is integrated by a Runge–Kutta–Fehlberg scheme featuring an automatic time-step control. The computation and superposition of a large number of droplet trajectories results in a smooth and continuous flow field of the disperse liquid phase in a statistical sense: Increasing the number of trajectories leads to a reduction of the variance of the liquid-phase flow variables.

5. Spray/wall and spray/film interaction

In many two-phase flow applications, interactions between droplets and flow boundaries have a decisive influence on the overall flow behavior. In the case of the LPP premix duct, interaction between the spray and the wall and the wall film significantly affects the fuel distribution in the flow entering the combustion zone. Thus, a comprehensive modeling of the droplet impact process is indispensable for a realistic simulation of the two-phase flow close to the wall. The mechanisms for a dry wall were investigated experimentally by several groups in the past (Stow and Stainer, 1977; Walzel, 1980; Samenfink, 1997; Coghe et al., 1995). For a detailed simulation, the interaction mechanisms have to be classified with respect to the conditions on the wall and the impact parameters of the droplet. The first level of classification distinguishes between a dry wall and a liquid wall film. Droplet impact on a dry wall is further divided into three characteristic wall temperature regimes: *Cold wall* – a temperature well below the fluid boiling temperature, *moderately hot wall* – a transition range up to a modified Leidenfrost temperature and *hot wall* – a temperature well above the modified Leidenfrost temperature (see Fig. 3).

5.1. Dry wall with $T \leqslant 1.05T_\mathrm{b}$

For wall temperatures up to approximately $1.05\,T_\mathrm{b}$, the cold–wall interaction mechanisms are dominating (Samenfink, 1997). In this temperature regime, the two possible interaction mechanisms are either splashing or complete deposition of the droplet. In the case of splashing, a fraction of the droplet mass is deposited on the wall whereas the remainder is ejected back into the gas flow decomposed into secondary droplets. A possible approach to distinguish between splashing and complete deposition involves the impact Reynolds number and the Laplace number,

$$\mathrm{Re} = \frac{u_\mathrm{n}D\rho_\mathrm{d}}{\mu_\mathrm{d}} \quad \text{and} \quad \mathrm{La} = \frac{D\sigma_\mathrm{d}\rho_\mathrm{d}}{\mu_\mathrm{d}^2}. \tag{15}$$

The impact Reynolds number is based on a corrected droplet velocity normal to the wall $u_\mathrm{n} = u_\mathrm{d}\sin\alpha^{0.63}$. With respect to a Re–La map, an analysis of numerous droplet

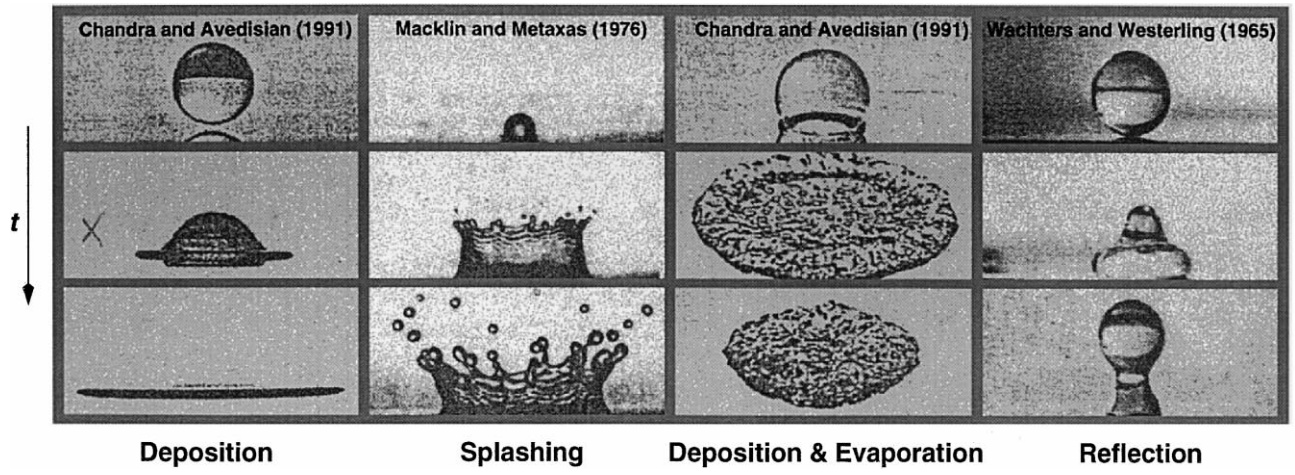

Fig. 3. Visualizations of droplet/wall interaction mechanism.

impact experiments indicates that splashing is separated from complete deposition by the function

$$\mathrm{Re} = 24\,\mathrm{La}^{0.419}, \tag{16}$$

represented by the bold line in Fig. 4a. In order to quantify the splashing process, it is necessary to establish a relation for the deposition rate η characterizing the fraction of the deposited droplet mass. Up to now, experimental studies reveal only little information about the details of the splashing process and the deposition rate. However, it is evident from several studies by Weiß (1993), Stow and Stainer (1977) and Mundo et al. (1995), that the distance from the splashing/deposition separation line in the logarithmic Re–La plane has a dominating influence on the deposition rate in the splashing domain Analytically, the distance from the splashing/deposition separation line can be described by the splashing parameter S expressed by the relation

$$\mathrm{Re} = S\,24\,\mathrm{La}^{0.419}, \tag{17}$$

where $S = 1$ represents zero distance. Because the splashing process is insufficiently understood, a practical approach is chosen in this study which is based on an extrapolation of experiments on the interaction of droplets with thin wavy films by Samenfink (1997)

$$\eta = S^{-0.6}. \tag{18}$$

Local sources of fuel mass, momentum and enthalpy for the liquid wall film are determined as follows

$$S_{\mathrm{m}} = \eta\,\mathrm{Tr}\,m_{\mathrm{d}}, \quad S_{\vec{u}} = \eta\,\mathrm{Tr}\,m_{\mathrm{d}}\vec{u}_{\mathrm{d}}, \quad S_{\mathrm{T}} = \eta\,\mathrm{Tr}\,m_{\mathrm{d}}h_{\mathrm{d}}. \tag{19}$$

In these expressions, Tr represents the droplet rate, determining the droplet number flux assigned to an individual trajectory of the spray.

A second important part of the modeling of the splashing process addresses the determination of initial conditions for secondary droplets. Secondary droplets have much smaller diameters compared to their parent droplet. The diameter distribution of the droplet cloud produced by splashing follows a log-normal distribution

$$P(D) = \frac{1}{\sqrt{2\pi}x\sigma}\exp\left[-\frac{(x-\bar{x})^2}{2\sigma^2}\right], \quad x = \ln D. \tag{20}$$

Based on data extracted from the literature, a relation for the diameter parameter $\bar{x} = \ln D_{\mathrm{m}}$ in the log-normal distribution can be derived in satisfying agreement with the experimental work by Samenfink (1997) and Stow and Stainer (1977)

$$\ln\frac{D_{\mathrm{m}}}{D_0} = -2 - \frac{D_0}{D_{\mathrm{ref}}} - 0.05\,S, \quad D_{\mathrm{ref}} = 4066\,\mu\mathrm{m}. \tag{21}$$

In this relation, D_0 denotes the droplet diameter just before impact. Obviously, this correlation is not based on physical reasoning but rather achieves experimental agreement for the total range of gas-turbine applications. The width of the diameter distribution slightly increases with an increasing splashing parameter S. Due to the limited available experimental data, the constant value 0.45 for the variance parameter σ is assumed in this study. Ejection angles of the secondary droplets are typically in the range of $\alpha = 10°$ to $\alpha = 15°$ relative to the wall whereas initial velocities are about 60% of the impact value. In combustor applications, secondary droplets from splashing are very tiny and instantly follow the gas flow in the near-wall region. Therefore, a detailed modeling of initial velocity and position is not necessary for the secondary droplets.

5.2. Dry wall with $1.05\,T_{\mathrm{b}} \leqslant T < T_{\mathrm{L}}^{*}$

Increasing the wall temperature from $1.05\,T_{\mathrm{b}}$ up to a modified Leidenfrost temperature, a number of various complex phenomena are observed. Surface roughness peaks penetrate the thin vapor film between droplet and wall and enhance the heat transfer into the droplet. Several transition states from splashing, disruption into smallest secondary droplet fragments,instant evaporation to local boiling are identified. To simplify the modeling of all these phenomena, instant evaporation is considered as the representative mechanism for this wall-temperature range. The upper limit of this temperature range is derived from several measurements of droplet impacts on a hot surface varying size, temperature and incident velocity of the droplets. An analysis of these experiments indicates the following modified Leidenfrost temperature which is dependent on liquid properties and impact velocity

$$\frac{T_{\mathrm{L}}^{*} - T_{\mathrm{L}}}{T_{\mathrm{L}}} = 0.027\sqrt{\mathrm{We}_{\mathrm{d}}}. \tag{22}$$

5.3. Dry wall with $T > T_{\mathrm{L}}^{*}$

On very hot walls, the determining interaction mechanism is reflection. Several authors have derived equations for the

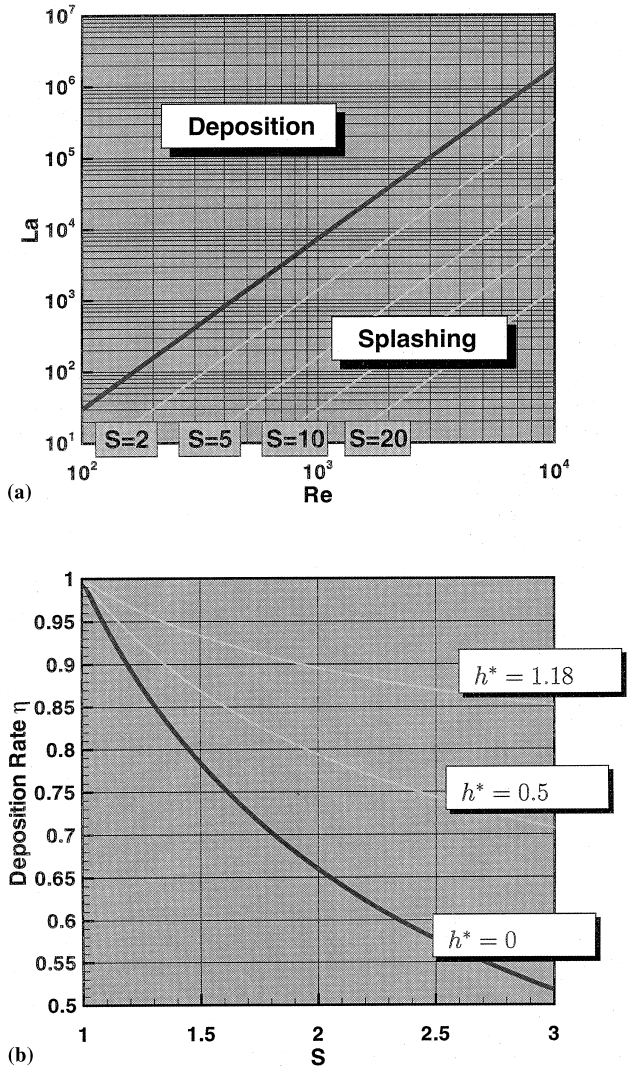

Fig. 4. (a) Re–La plane for the cold wall. (b) Deposition rate η for wall film.

diameter change due to the formation of a vapor film (Li et al., 1995; Wachters and Westerling, 1966). For flow conditions in combustors, this diameter decrease is of minor importance and is consequently neglected. Because of a very short interaction time and an isolating effect of the vapor cushion, the energy transport to the droplet during the interaction time has no significant effect. The change of the wall normal velocity component due to the reflection can be described by the following equation

$$\frac{u_{n,1}}{u_{n,0}} = \sqrt{1 - 37\,We^{0.25}\,On.} \tag{23}$$

5.4. Wall covered with liquid film

Basically, the mechanisms of interaction do not change in the presence of a liquid film. By analogy with the cold dry wall case described above, the separation line dividing the splashing and deposition domain is described by Eq. (16). For typical thin films in combustor flows ($h_f < 150$ μm), film thickness has no significant influence on the splashing/deposition border. However, a decisive influence is observed on the deposition rate η. The following correlation can be deduced from the experimental data of Samenfink (1997)

$$1 - \eta_{film} = (1 - \eta_{drywall}) \exp(-h^*), \quad h^* = \frac{h_f}{D_0}. \tag{24}$$

From this correlation, it is obvious that a thicker film leads to an enlarged deposition rate by damping the splashing process as illustrated in Fig. 4b.

5.5. Computation of secondary droplets

In order to simulate a spray generated by an atomizer, only a limited number of individual droplets with different initial conditions are tracked. The larger this number and the finer the discretization of the spectrum of initial conditions, the more realistic the simulation of the atomization process. In a similar way, a splashing event is simulated only by a limited number of representative secondary droplets. Consistent with the stochastic concept of the Lagrangian approach, the initial conditions of the secondary droplets are determined by a random procedure. In the present flow calculation, ten to twenty secondary droplets have been generated to simulate a splashing droplet.

6. Wall film propagation and evaporation

The calculation of the film flow on the duct wall is based on a boundary layer description (Rosskamp et al., 1997). In this approach, the wavy wall film is developed in a plane and described in a time-averaged manner. Fig. 5a shows a schematic model film which represents all important integral characteristics of a shear driven film. The wavy film surface structure is taken into account by introducing an equivalent sand grain roughness $k_s = 2h_f \Psi$ (Himmelsbach et al., 1994). In this relation, Ψ is a correction factor taking into account the change in surface structure as the shear stress at the liquid/gas interface increases. For many liquids with a viscosity and surface tension similar to water, alcohols or hydrocarbon fuels this factor is calculated from $\Psi = 0.735 + 0.09255[1/\mathrm{Pa}]\tau_s$. The internal temperature profile of the model film is determined from a superposition of a rapid mixing zone and a laminar sublayer zone (Rosskamp et al., 1997). This temperature profile is used to calculate variable thermo-physical fluid properties. Conservation of energy is implemented in terms of an enthalpy balance on the control volume indicated in Fig. 5b. Based on these modeling assumptions, a set of three differential equations can be derived for mass transport, film surface speed and film temperature. In a similar way to the integration of the droplet trajectories, this system of equations is integrated in the film-propagation direction by means of a Runge–Kutta method featuring a self-adapting step size.

7. Coupled solution of gas flow, spray and film flow

As described above, the flow regimes of gas phase, wall film and spray are interacting by means of mass, momentum and energy transfer. With respect to Fig. 2 the computation of the film flow is implemented directly into the pressure based, block-iterative solution procedure of the gas-phase flow field in the program EPOS. In the present simulation, individual film-flow solutions are calculated every 50th non-linear iteration of the gas flow solution procedure, each time returning updates for the source term fields due to film flow and evaporation. In this way, a simultaneous solution of the gas-flow field and wall-film flow field is obtained. Designed as a post processing-processing

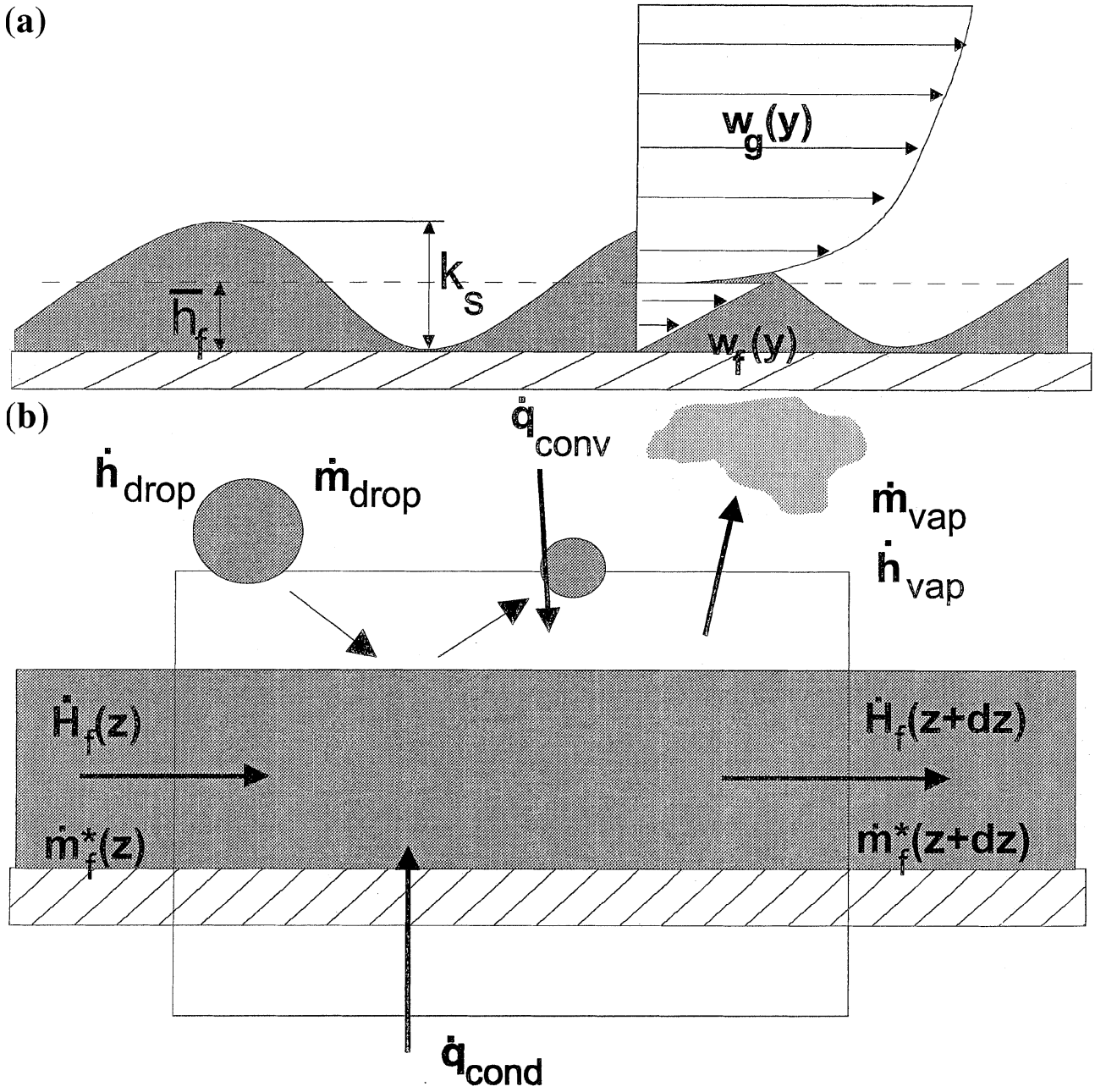

Fig. 5. (a) Model for the the shear driven wall film. (b) Control volume for mass and enthalpy fluxes.

unit to EPOS, the program Ladrop computes dispersion and evaporation of the spray including secondary droplets from splashing. As a result, Ladrop returns droplet source term fields for the gas and film flow solution in the next EPOS/Ladrop iteration. Because of the intense interdependence of spray and gas flow in the present calculation, a special relaxation strategy has to be applied for the gas phase droplet source fields

$$\overline{S}^i_{d,\phi} = \alpha S^i_{d,\phi} + (1-\alpha)\overline{S}^{i-1}_{d,\phi}, \tag{25}$$

with the source term $S^i_{d,\phi}$ calculated by Ladrop and the source term $\overline{S}^i_{d,\phi}$ actually used in the gas flow calculation according to Eq. (2). In particular, the enthalpy source fields caused by evaporation are prone to excessive oscillations during the iteration procedure. Effectively, a relaxation factor $\alpha = 0.05$ has to be chosen in order to assure a stable iteration procedure. As a consequence, 130 EPOS/Ladrop iterations have been necessary to completely account for the droplet source terms. Being a characteristic integral quantity, the total evaporated fuel mass fraction is used as a criterion to assess the convergence of the solution.

8. Results

8.1. Example geometry

The test case is a schematic arrangement of an atomizer in a premix duct basically similar to the sketch in Fig. 1. It was chosen as a representative two-phase flow case with a significant influence of the evaporating liquid phase on the overall

Table 1
Parameters of the premix duct test case

r_a (m)	l_{duct} (m)	$\dot{m}_{air}$ (kg/s)	$\dot{m}_{fuel}$ (kg/s)	T_{air} (K)	p_{air} (Pa)	T_{fuel} (K)	Φ_{global} (−)
0.023	0.11	0.25	0.00866	658	500 000	300	0.5

flow structure. Table 1 summarizes the most important test case parameters. A hollow-cone pressure atomizer with 100° spray cone angle is used to atomize tetradecane, a diesel fuel substitute. The initial diameter spectrum of the spray is represented by ten diameter classes and follows a Rosin–Rammler distribution of $D_{63} = 60\,\mu m$ and $n = 1.5$.

The gas-flow plot in Fig. 2 illustrates the plain gas-phase solution, resulting from a computation with 8370 finite

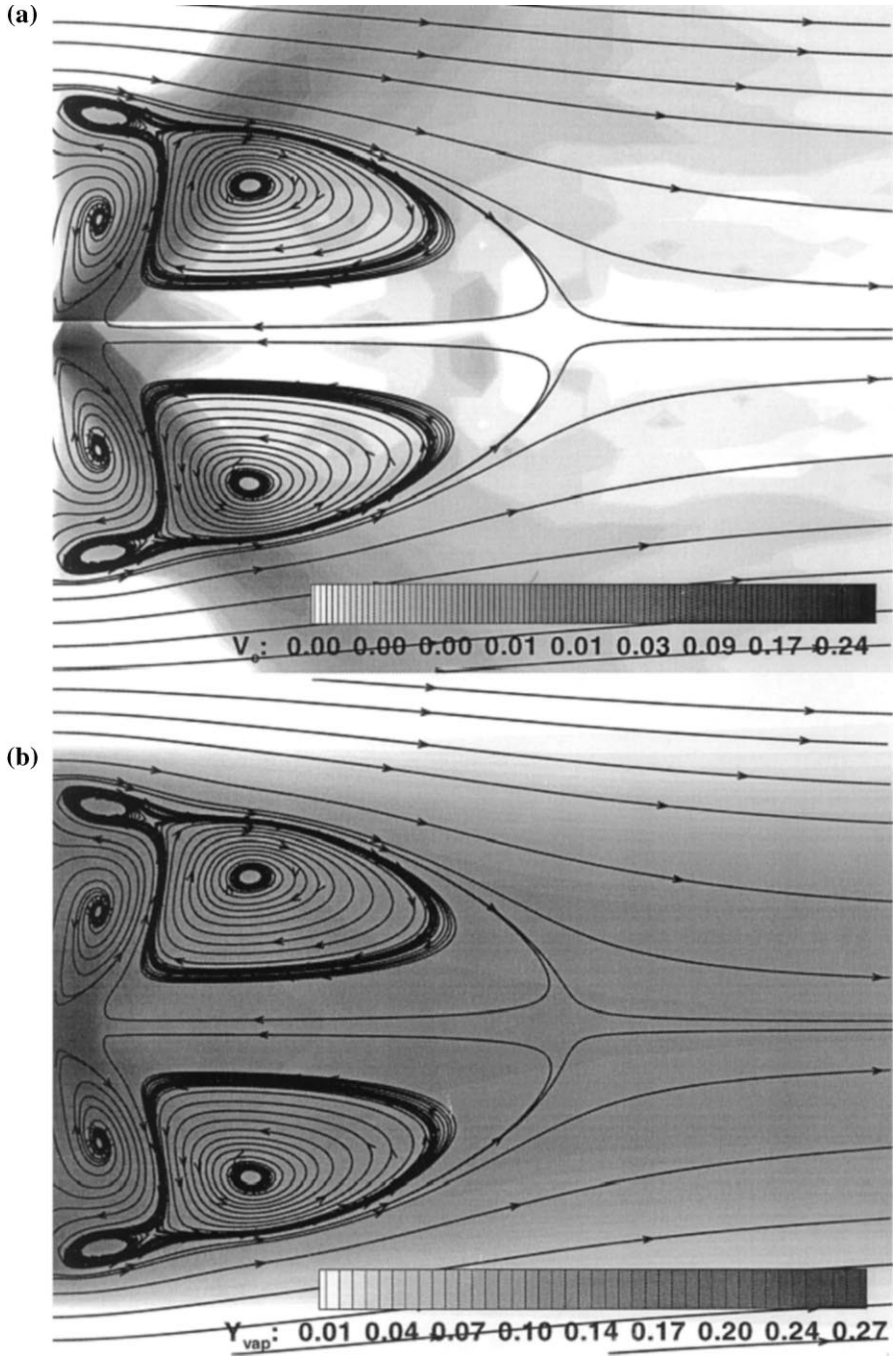

Fig. 6. (a) Streamlines and liquid volume concentration. (b) Streamlines and fuel vapor concentration.

volumes. It is taken as a reference solution to analyze the influence of the two-phase flow effects and to demonstrate the performance of the iterative two-phase flow approach presented in this study. The atomizer on the axis of the premix duct is creating a short recirculation zone with a rather small effect on the main flow. As illustrated in Fig. 1 the duct liner is surrounded by hot discharge air from the compressor and represents an adiabatic boundary for the gas flow.

8.2. Spray calculation without wall film and spray/wall interaction

In order to demonstrate the effect of gas flow/spray interaction, a flow field is calculated in a first step considering only spray dispersion and evaporation in addition to the gas flow. During the first 30 EPOS/Ladrop iterations, the two-phase flow field is changing significantly due to aerodynamic acceleration and evaporation cooling of the gas flow by the spray. Due to a total fuel evaporation of 26.5% in the flow field (see Fig. 7), the temperature of the gas flow on the duct axis is decreased by 100 K. The effect on the flow separation region behind the atomizer is illustrated in Fig. 6. The 100°-spray cone is clearly indicated by the contour plot of the liquid volume concentration. Due to the massive aerodynamic drag of the spray in the injection region, the simple recirculation zone of the plain air flow case (Fig. 2) is now split into three individual vortex structures (Fig. 6). The high vapor concentration in the inner vortex zone between atomizer and spray cone is constantly fed by vapor and the smallest droplets from the fuel nozzle. Due to its complete separation from the main flow by the two other vortices,the vapor accumulates in this vortex zone. A moderately high vapor concentration extends from the remaining part of the flow separation region downstream of the flow in the premix duct. In general, smaller droplets are dragged with the main flow, whereas larger droplets with a dominating inertia penetrate the main flow and hit the duct liner. Since no wall interaction and film formation is considered in this calculation, fuel evaporation and concentration are significantly underestimated in the near-wall region (see Fig. 7).

8.3. Spray calculation including wall and film interaction

Based on the preceding calculation, the models for spray/wall and spray/film interaction are now applied to simulate droplet impacts on a propagating and evaporating liquid wall film. As a consequence, the flow field is modified significantly in the region close to the duct wall. Representing a decisive fraction of the liquid fuel mass, the larger droplets of the spray penetrate the main flow and hit the liquid film on the duct wall. Depending on their impact parameters, they deposit on the film and/or produce clouds of tiny secondary droplets. The instantly dragged secondary droplets as well as the liquid film intensify the fuel evaporation in the near-wall region, increasing fuel concentration and decreasing gas temperature. As a result, the overall fuel evaporation is now raised to 30.8% of the injected fuel mass. Due to this additional region of intense fuel evaporation, the homogeneous distribution of fuel vapor in the premix duct is significantly improved. It is obvious, that the quality of the present flow simulation decisively depends on the advanced modeling of film propagation and evaporation in combination with sophisticated spray/wall and spray/film interaction models. Of particular importance is a realistic description of the deposition rate and the diameter distribution of secondary droplets due to splashing (see Fig. 8).

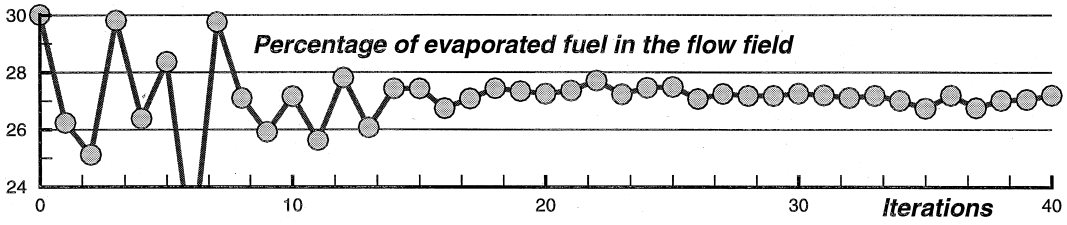

Fig. 7. History of the iterative solution procedure.

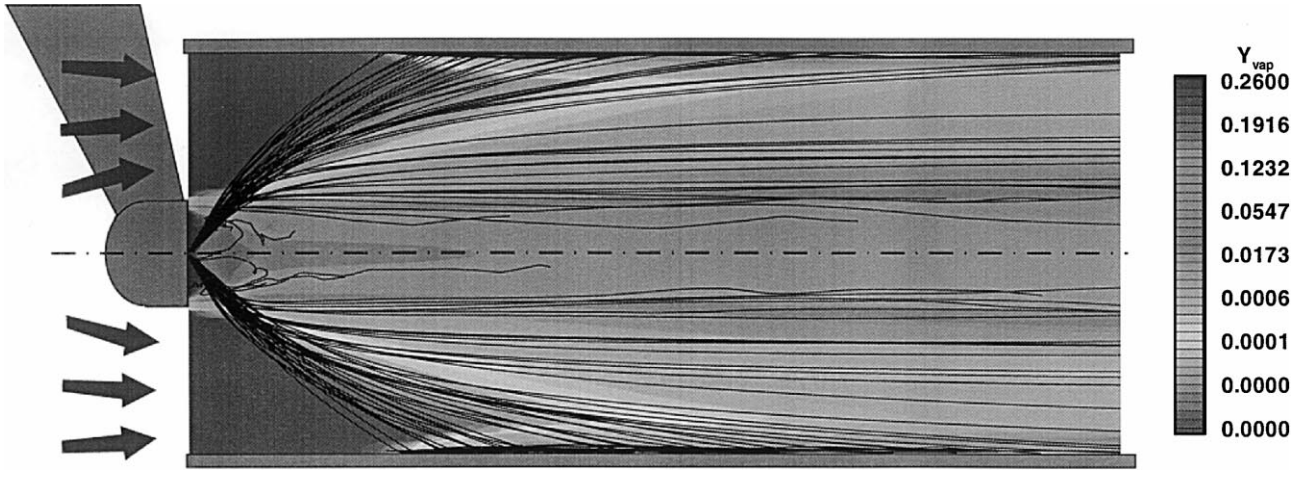

Fig. 8. Droplet trajectories and fuel vapor concentration in the premix duct.

9. Summary and conclusions

A new approach to the coupled solution of the interdependent flow fields of gas phase, spray and wall film has been presented in this paper. The iterative procedure comprises three individual sub-units. In a first step, the gas phase and liquid wall-film flow are simultaneously solved by means of a finite-volume method and a finite-difference method, respectively. In a second step, dispersion and evaporation of the fuel spray is computed using a Lagrangian particle tracking approach. The individual calculations of gas-phase flow, spray and film flow communicate by exchanging source fields for liquid and gaseous fuel. Due to the intense interaction between liquid and gas phase in the reported flow simulation, relaxation of the iterative solution procedure is required. To improve the quality of the flow simulation in the wall region of the flow, advanced spray/wall and spray/film interaction models are implemented in the particle tracking method. Based on various experimental studies, this paper provides a complete classification and description of droplet/wall and droplet/film interaction models necessary for the development of a computer code. Results of a flow simulation in a schematic premix duct demonstrate the effect of the phase interaction and emphasize the importance of a coupled solution of the two-phase flow. In addition, the test case illustrates the influence of realistic spray/wall and spray/film interaction modeling on the flow simulation in the wall region of the duct.

Acknowledgements

This work combines the results of recent developments within the ''Low Emission Combustor Technology Program'' of the European Community, within the ''Graduiertenkolleg Energie- und Umwelttechnik'' and within the ''Sonderforschungsbereich 167 – Hochbelastete Brennräume''. The financial support for these programs by the European Community (Contract AER2-CT-92-0036) and the Deutsche Forschungsgemeinschaft (DFG) is gratefully acknowledged.

References

Baumann, W., H. Bendisch, H. Eickhoff, Thiele, F., 1989. Interaction of hot swirling air and liquid film flow in air blast atomizers. In: International Symposium on Air Breathing Engines 971–976.

Coghe, A., G. Cossali, Marengo, M., 1995. A first study about single droplet impingement on thin liquid film in a low laplace number range. In: ICLASS-95, Nürnberg 285–293.

Gosman, A.D., Ioannides, E., 1983. Aspects of computer simulation of liquid-fueled combustors. Journal of Energy 7 (6), 482–490.

Himmelsbach, J., Noll, B., Wittig, S., 1994. Experimental and numerical studies of evaporating wavy fuel films in turbulent air flow. International Journal of Heat and Mass Transfer 37, 1217–1226.

Kays, W., Crawford,M., 1980. Convective Heat and Mass Transfer. McGraw-Hill, New York.

Kind, R., Yowakim, F., Sjolander, S., 1989. The law of the wall for swirling flow in annular ducts. Journal of Fluids Engineering 111, 160–164.

Kurreck, M., Willmann, M., Wittig, S., 1996. Prediction of the three-dimensional reacting two phase flow within a jet-stabilized combustor. ASME-Paper 96-GT-468.

Launder, B., Spalding, D., 1974. The numerical computation of turbulent flows. Computer Methods in Applied Mechanics and Engineering 3, 269–289.

Li, S., Libby, P., Williams, F., 1995. Spray impingement on a hot surface in reacting stagnation flows. AIAA Journal 33 (6), 1046–1055.

Milojević, D., 1990. Lagrangian stochastic-deterministic (LSD) predictions of particle dispersion in turbulence. Particle and Particle Systems Characterization 7, 181–190.

Mundo, C., Sommerfeld, M., Tropea, C., 1995. Droplet-wall collisions: Experimental studies of the deformation and breakup process. International Journal of Multiphase Flow 21 (2), 151–174.

Noll, B., Bauer, H.-J., Wittig, S., 1991. Generalized conjugate gradient method for the efficient solution of three-dimensional fluid flow problems. Numerical Heat Transfer 20, 207–221.

Rosskamp, H., Willmann, M., Wittig, S. (9–12. June 1997). Heat up and evaporation of shear driven liquid wall films in hot turbulent air flow. In: Proceedings of the 2nd International Symposium on Turbulence, Heat and Mass Transfer, Delft, The Netherlands.

Samenfink, W., 1997. Grundlegende Untersuchung zur Tropfeninteraktion mit schubspannungsgetriebenen Wandfilmen. Ph.D. thesis, Universität Karlsruhe.

Sill, K., 1982. Wärme- und Stoffübertragung inturbulenten Strömungsgrenzschichten längs verdunstender welliger Wasserfilme. Ph.D. thesis, Universität Karlsruhe.

Sparrow, E.M., Gregg, J.L., 1958. The variable fluid property problem in free convection. Transactions of the ASME 80, 879–886.

Stein, W., 1973. Berechnung der Verdampfung von Flüssigkeit aus feuchten Produkten in Sprühturm. Verfahrenstechnik 7(9).

Stow, C., Stainer, R., 1977. The physical products of a splashing water drop. Journal of the Meteorological Society of Japan 55 (5), 518–531.

Tolpadi, A.K., 1995. Calculation of two-phase flow in gas turbine combustors. ASME – Journal of Engineering for Gas Turbines and Power 117, 695–703.

Tolpadi, A.K., Burrus, D.L., Lawson, R.J., 1995. Numerical computation and validation of two-phase flow downstream of a gas turbine dome swirl cup. ASME – Journal of Engineering for Gas Turbines and Power 117, 704–712.

Van Doormal, J.P., Raithby, G.D., 1984. Enhancement of the SIMPLE method for predicting incompressible fluid plows. Numerical Heat Transfer 7, 147–163.

Wachters, L., Westerling, N., 1966. The heat transfer from a hot wall to impinging water drops in the spheroidal state. Chemical Engineering Science 21, 1047–1056.

Walzel, P., 1980. Zerteilgrenze beim Tropfenzerfall. Chemie-Ingenieur-Technik 52, 338–339.

Weiß, D., 1993. Periodischer Aufprall monodisperser Tropfen gliecher Geschwingkeit auf feste Oberflächen. Ph.D. thesis, Univesität Göttingen.

Wittig, S., Himmelsbach, J., Noll, B., Feld, H., 1991. Motion and evaporation of shear driven liquid films in turbulent gases. ASME-Paper 91-GT-207.